ACS APPLIED BIO MATERIALS

www.acsabm.org Article

Syntheses and Applications of Coumarin-Derived Fluorescent Probes for Real-Time Monitoring of NAD(P)H Dynamics in Living Cells across Diverse Chemical Environments

Adenike Mary Olowolagba, Micah Olamide Idowu, Dilka Liyana Arachchige, Omowunmi Rebecca Aworinde, Sushil K. Dwivedi,* Olivya Rose Graham, Thomas Werner, Rudy L. Luck,* and Haiying Liu*

Cite This: *ACS Appl. Bio Mater.* 2024, 7, 5437−5451 Read Online

ACCESS | Metrics & More | Article Recommendations | Supporting Information

ABSTRACT: Fluorescent probes play a crucial role in elucidating cellular processes, with NAD(P)H sensing being pivotal in understanding cellular metabolism and redox biology. Here, the development and characterization of three fluorescent probes, **A**, **B**, and **C**, based on the coumarin platform for monitoring of NAD(P)H levels in living cells are described. Probes **A** and **B** incorporate a coumarin-cyanine hybrid structure with vinyl and thiophene connection bridges to 3-quinolinium acceptors, respectively, while probe **C** introduces a dicyano moiety for replacement of the lactone carbonyl group of probe **A** which increases the reaction rate of the probe with NAD(P)H. Initially, all probes exhibit subdued fluorescence due to intramolecular charge transfer (ICT) quenching. However, upon hydride transfer by NAD(P)H, fluorescence activation is triggered through enhanced ICT. Theoretical calculations confirm that the electronic absorption changes upon the addition of hydride to originate from the quinoline moiety instead of the coumarin section and end up in the middle section, illustrating how the addition of hydride affects the nature of this absorption. Control and dose−response experiments provide conclusive evidence of probe **C**'s specificity and reliability in identifying intracellular NAD(P)H levels within HeLa cells. Furthermore, colocalization studies indicate probe **C**'s selective targeting of mitochondria. Investigation into metabolic substrates reveals the influence of glucose, maltose, pyruvate, lactate, acesulfame potassium, and aspartame on NAD(P)H levels, shedding light on cellular responses to nutrient availability and artificial sweeteners. Additionally, we explore the consequence of oxaliplatin on cellular NAD(P)H levels, revealing complex interplays between DNA damage repair, metabolic reprogramming, and enzyme activities. In vivo studies utilizing starved fruit fly larvae underscore probe **C**'s efficacy in monitoring NAD(P)H dynamics in response to external compounds. These findings highlight probe **C**'s utility as a versatile tool for investigating NAD(P)H signaling pathways in biomedical research contexts, offering insights into cellular metabolism, stress responses, and disease mechanisms.

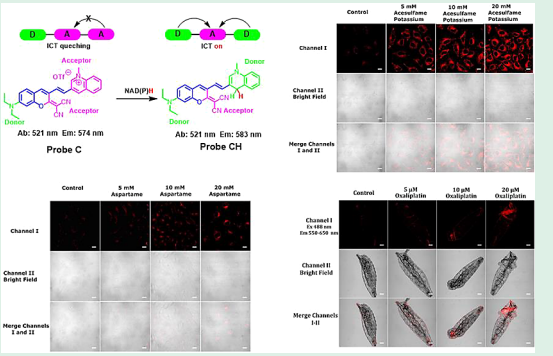

KEYWORDS: *NAD(P)H, fluorescent probes, coumarin, artificial sugars, cellular imaging, cyanine dyes*

1. INTRODUCTION

NADH (1,4-Dihydronicotinamide Adenine Dinucleotide) and NADPH (1,4-Dihydronicotinamide Adenine Dinucleotide Phosphate) are coenzymes, jointly referred to as NAD(P)H,[1] that are crucial for energy metabolism, gene expression regulation, and redox signaling pathways.[2−4] NADH is a cofactor for various enzymes involved in metabolism and gene expression regulation and also functions as a carrier of electrons for the transport chain in mitochondria.[2−4] Proper NADH levels are essential for maintaining mitochondrial function and cellular redox balance.[2−4] Conversely, NADPH is crucial for cellular defense against reactive oxygen species (ROS) and is involved in detoxifying ROS, biosynthetic pathways, and neurotransmitter production.[5,6] Reduced NADPH levels are linked to impaired insulin secretion and glucose metabolism, resulting in type 2 diabetes.[7] Reduced NADPH levels can also lead to increased ROS production, causing cell death from DNA damage and oxidative stress, and, contributing to the formation of various diseases.[8] Developing sensitive and specific methods to detect and quantify NAD(P)H in live cells has broad implications for improving our understanding of the molecular mechanisms that underlie various physiological and pathological processes.[9−12] These

Received: May 1, 2024
Revised: June 25, 2024
Accepted: July 1, 2024
Published: July 12, 2024

https://doi.org/10.1021/acsabm.4c00595
ACS Appl. Bio Mater. 2024, 7, 5437−5451

Scheme 1. Coumarin-Based Fluorescent Probes for Biosensing of NAD(P)H

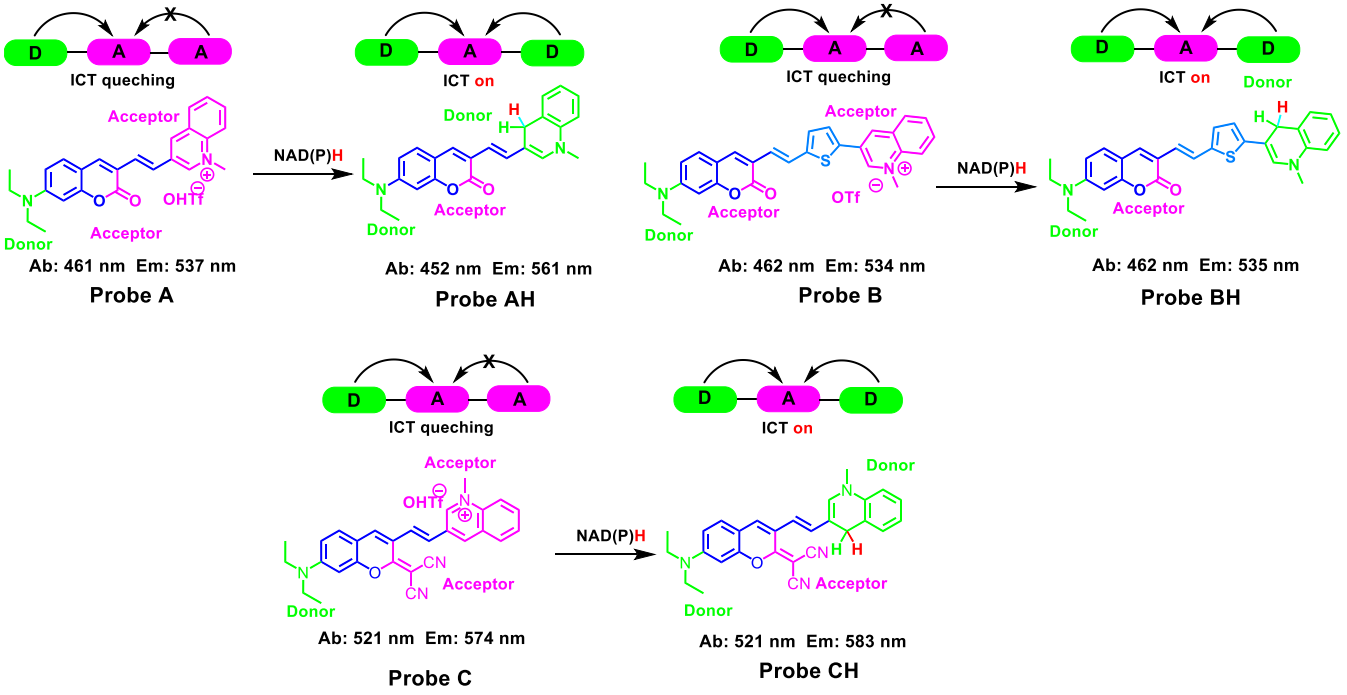

methods can also aid in early disease diagnosis and prognosis, and the development of targeted therapeutic strategies.[9−12] Ultimately, advances in the detection and quantification of NAD(P)H can lead to improved patient outcomes and a better understanding of the molecular mechanisms underlying various diseases.[9−12] Fluorescence imaging with fluorescent probes is a valuable technique for assessing NAD(P)H in live cells.[9−21] This technique has several advantages over other methods, including high sensitivity, specificity, and noninvasiveness. It also allows for live-cell imaging, enabling the monitoring of changes in NAD(P)H in real-time.[9−22] Furthermore, fluorescence imaging with fluorescent probes enables multiplexing, which means that multiple targets can be detected simultaneously.[9−24] This technique also allows for high throughput screening, which can identify compounds that affect NAD(P)H metabolism.[9−24] As a result, fluorescence imaging with fluorescent probes is a powerful tool for studying the molecular mechanisms underlying various physiological and pathological processes, as well as for developing new therapeutic strategies.[9−21,23,24] Developing fluorescent probes with longer emission wavelengths is critical for reducing the interference from the intrinsic fluorescence properties of NAD(P)H, minimizing signal attenuation, enhancing imaging resolution through deeper tissue penetration of light, and improving the accuracy and sensitivity of fluorescence imaging in live cells.[9−21,23,24]

Our probe formulations are based upon coumarins which are a large family of 2H-chromen-2-one-containing compounds that are widely used as fluorescent fluorophores due to their unique optical and chemical properties, including broad excitation and emission wavelengths, high quantum yield, chemical stability, low toxicity, and ease of modification.[25−29] As a result, coumarins are utilized as a desirable and ideal fluorophore platform for a wide range of applications, such as biological imaging, sensing, and diagnostics for cations,[30] anions,[27,29,31] pH,[32−34] NADH,[17] H_2S,[27,29,31] cysteine, homocysteine, and glutathione (GSH),[27,29,31] cellular membranes, and reactive oxygen and nitrogen species.[27,29,31,35,36] The fluorescence of coumarin fluorophores has been tuned to longer emission regions by extending the π-conjugation at the 3- or 4-position through a vinyl or single carbon−carbon bond connection to different aromatic groups,[17,25,37,38] replacing the carbonyl group on the lactone moiety of the coumarin dyes with 4-pyridylacetonitrile and cyano(4-nitrophenyl)methylene moieties,[39−42] and by forming fused rhodamine dyes.[34,43−46] A deep-red coumarin-based fluorescent probe has recently been developed for NADH-sensing applications by introducing a quinolinium moiety at the 3-position of coumarin through a vinyl bond and replacing the lactone carbonyl group with a dicyano group.[17] In this study, we present the synthesis and characterization of three novel fluorescent probes (**A**, **B**, and **C**) designed specifically for the detection of NAD(P)H in live cells. Our investigation focuses on elucidating how the chemical structures of these probes influence their optical properties, sensitivity, and fluorescence responses to NAD(P)H, aiming to identify the most effective probe for monitoring NAD(P)H levels in cells treated with artificial sweeteners. By exploring these relationships, we aim to provide practical insights that can guide the development of more efficient fluorescent probes for NAD(P)H sensing applications (Scheme 1). Probes **A** and **B** feature a coumarin-cyanine hybrid structure interconnected by vinyl and thiophene bridges, leading to 3-quinolinium acceptors. In contrast, Probe **C** replaces the coumarin carbonyl group in Probe A with a dicyano moiety, significantly enhancing its electron-withdrawing capacity. This modification augments the reactivity of the 3-quinolinium moiety toward NAD(P)H, thereby accelerating the reaction kinetics. This strategic design ensures that the probes exhibit rapid responsiveness, high specificity, and reliable performance in detecting intracellular NAD(P)H levels. Initial investigations into probe **A** and probe **B** elucidate the subtleties of their fluorescence behavior, characterized by intramolecular charge transfer (ICT) quenching in their basal states. However, upon interaction

https://doi.org/10.1021/acsabm.4c00595
ACS Appl. Bio Mater. 2024, 7, 5437−5451

Scheme 2. Synthetic Strategy to Produce Coumarin-Based Probes A–C for NAD(P)H Sensing

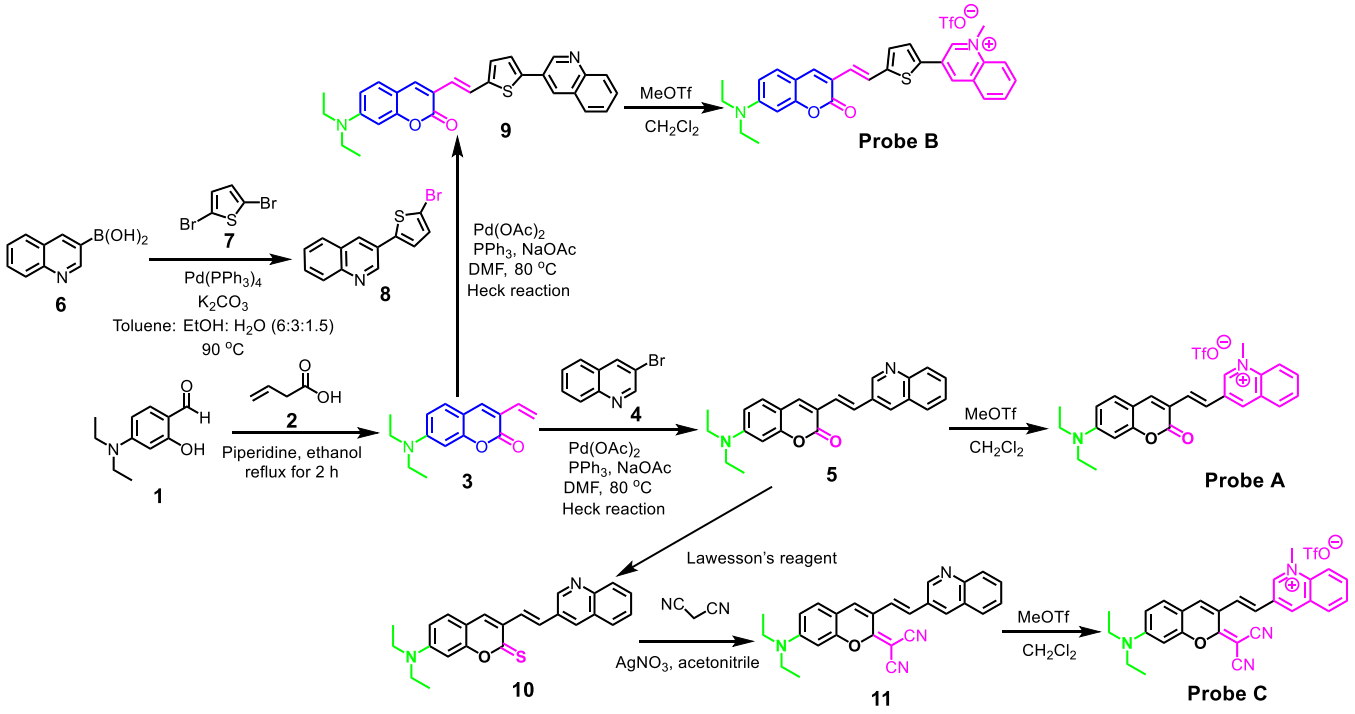

with NAD(P)H, fluorescence activation is triggered through enhanced ICT, demonstrating the potential utility of these probes for real-time NAD(P)H sensing. Probe **C** emerges as a promising candidate for dynamic monitoring of cellular NAD(P)H levels due to its rapid responsiveness and turn-on longer wavelength emission. Furthermore, the selective targeting of mitochondria by probe **C** underscores its potential for probing mitochondrial redox metabolism and energy homeostasis. Beyond probe development, our study investigates the impact of metabolic substrates, artificial sweeteners, and chemotherapeutic agents on cellular NAD(P)H levels (Scheme 1). Through experimentation with HeLa cells and in vivo studies using starved fruit fly larvae, we elucidate the intricate interplays between cellular metabolism, stress responses, and disease mechanisms. In summary, our investigation into the development of fluorescent probes for NAD(P)H determinations holds promise for advancing the understanding of cellular metabolism, redox biology, and disease pathogenesis.

2. EXPERIMENTAL SECTION

2.1. Instrumentation. The NMR spectra (^{1}H at 500 MHz and ^{13}C at 125 MHz) were acquired employing a Bruker NMR spectrometer (Ascend 500) in both DMSO-d_6 and $CDCl_3$ solvents at a concentration of 2.0×10^{-2} M. Absorption and emission spectra of the probes were examined using a PerkinElmer Lambda 35 UV/vis spectrometer and a Jobin Yvon Fluoromax-4 spectrofluorometer, respectively. For the mass spectrometry analysis of the probes and their reduced products, a Thermo Scientific LCQ Fleet mass spectrometer was utilized. Confocal imaging was conducted utilizing an OLYMPUS FLUOVIEW FV1000, followed by processing of the captured images using both ImageJ and GIMP 2.10 software. Prior to analysis, stock solutions of probe **A**, probe **B**, probe **C**, NADH, NADPH, and other relevant analytes were prepared in pH 7.4 phosphate-buffered saline.

2.2. Synthesis of Fluorescent Probes. *2.2.1. Synthesis of Probe A.* Methyl trifluoromethanesulfonate (57.9 μL, 1.2 equiv) was introduced into a solution containing compound **5** (158.0 mg, 0.043 mmol) dissolved in 10.0 mL of anhydrous dichloromethane at ambient temperature under an inert atmosphere. This mixture was stirred vigorously overnight. Subsequently, a discernible precipitate materialized. This precipitate was isolated by filtration, followed by thorough washing with dichloromethane, culminating in the acquisition of probe **A**. ^{1}H NMR (DMSO-d_6, 500 MHz): δ 9.85 (s, 1H), 9.30 (s, 1H), 8.44 (d, J = 10 Hz, 1H), 8.36 (d, J = 10 Hz, 1H), 8.17 (t, J = 7.5 Hz, 1H), 8.12 (s, 1H), 8.00 (t, J = 7.5 Hz, 1H), 7.75 (d, J = 15 Hz, 1H), 7.55 (m, 2H), 6.78 (d, J = 5.0 Hz, 1H), 6.58 (s, 1H), 4.64 (s, 3H), 3.46 (m, 4H), 1.14 (t, J = 7.5 Hz, 6H) ppm. ^{13}C NMR (DMSO-d_6, 125 MHz): δ 160.42, 156.21, 151.66, 149.72, 142.87, 141.17, 137.28, 134.90, 132.44, 130.64, 130.57, 130.30, 129.72, 122.58, 122.42, 119.86, 119.53, 115.02, 110.21, 108.73, 96.72, 45.87, 44.75, 12.83 ppm. MS/Z = 385.14.

2.2.2. Synthesis of Probe B. Compound **9** (187 mg, 0.41 mmol) was dissolved in 10 mL of dichloromethane, followed by the addition of methyl trifluoromethanesulfonate (51.4 μL, 0.454 mmol). The resulting mixture was stirred overnight under a nitrogen atmosphere at room temperature, yielding probe **B**. ^{1}H NMR (DMSO-d_6, 500 MHz): δ 9.96 (s, 1H),9.38 (s, 1H), 8.42 (m, 2H), 8.18 (t, J = 7.5 Hz, 1H), 8.09 (s, 1H), 8.02 (t, J = 7.5 Hz, 1H), 7.90 (d, J = 5.0 Hz, 1H), 7.70 (d, J = 15 Hz, 1H), 7.45 (d, J = 10 Hz, 1H), 7.39 (s, 1H), 6.96 (d, J = 15 Hz, 1H), 6.74 (d, J = 10 Hz, 1H), 6.55 (s, 1H), 4.68 (s, 1H), 3.44 (m, 4H), 1.13 (t, J = 7.5 Hz, 6H) ppm. ^{13}C NMR (DMSO-d_6, 125 MHz): δ 160.59, 155.83, 151.19, 148.36, 146.53, 140.61, 139.76, 137.20, 134.84, 130.87, 130.68, 130.11, 129.76, 129.13,128.61, 128.27, 125.48, 122.09, 119.54, 115.45, 110.03, 108.85, 96.73, 45.90, 44.65, 12.86 ppm. MS/Z = 467.26.

2.2.3. Synthesis of Probe C. Compound **11**, dissolved in dichloromethane (30 mg, 0.07 mmol), underwent a reaction upon the addition of methyl trifluoro methanesulfonate (8.23 μL, 0.073 mmol). The resulting mixture was stirred at room temperature under a nitrogen atmosphere overnight, yielding probe **C**. ^{1}H NMR (DMSO-d_6, 500 MHz): δ 9.74 (s, 1H), 9.32 (s, 1H), 8.48 (d, J = 10 Hz, 1H), 8.40 (d, J = 10 Hz, 1H), 8.23 (t, J = 7.5 Hz, 1H), 8.13 (s, 1H), 8.04 (t, J = 7.5 Hz, 1H), 7.86 (d, J = 15 Hz, 1H), 7.62 (d, J = 10 Hz, 1H), 7.26 (d, J = 15 Hz, 1H), 6.96 (d, J = 10 Hz, 1H), 6.64 (s, 1H), 4.67 (s, 3H), 3.53 (m, 4H), 1.17 (t, J = 7.5 Hz, 6H) ppm. ^{13}C NMR (DMSO-d_6, 125 MHz): δ 170.29, 155.15, 152.98, 149.42, 142.00, 140.10, 137.79, 131.28, 131.26, 130.91, 130.75, 129.62,

https://doi.org/10.1021/acsabm.4c00595
ACS Appl. Bio Mater. 2024, 7, 5437−5451

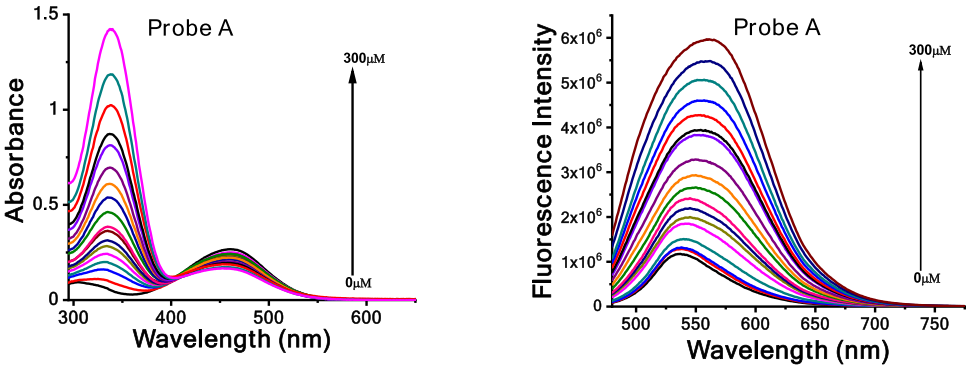

Figure 1. Absorption and fluorescence spectra of 10 μM probe **A** (304 and 461 nm) in the absence and presence of different NADH concentrations in pH 7.4 phosphate buffers under an excitation of 460 nm.

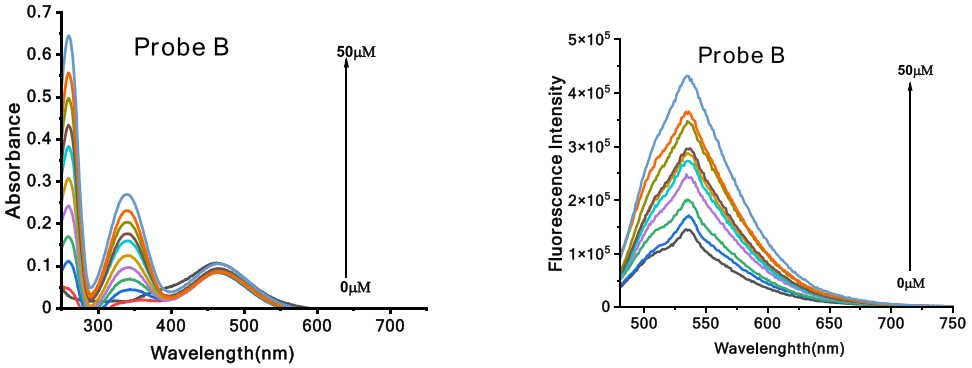

Figure 2. Absorption and fluorescence spectra of 10 μM probe **B** (465 nm) in the absence and presence of different NADH concentrations in pH 7.4 phosphate buffers under an excitation of 450 nm.

128.60, 125.25, 119.73, 117.25, 115.52, 112.58, 110.51, 95.99, 53.37, 53.04, 49.06, 46.23, 45.00, 12.81 ppm. MS/Z = 433.26.

2.2.4. Theoretical Calculations. Computer modeling of the probes was conducted following previously published protocols to establish their initial geometries.[47] Molecular data underwent refinement using density functional theory (DFT) with the APFD functional[48] and electron basis sets at the 6-311*g(d,p) level until convergence, within Gaussian 16[49] and utilizing a polarizable continuum model (PCM)[50] for water. Frequency calculations did not contain imaginary frequencies. Excited states were evaluated via TD-DFT optimization[51] employing the CAM-B3LYP functional[52] within a PCM of water. The results were analyzed using GaussView 6,[53] and all data and figures are detailed in the Electronic Supporting Information (ESI), including illustrations of LCAOs for all discussed molecular orbitals.

3. RESULTS AND DISCUSSION

3.1. Probe Design and Synthesis. The array of desirable characteristics exhibited by coumarin, including its unique combination of fluorescence properties, chemical stability, synthetic versatility, biocompatibility, and minimal background fluorescence, renders it useful for the construction of fluorescent probes that can detect NAD(P)H.[25−29] In line with this rationale, we methodically designed and synthesized two distinct fluorescent probes (probes **A** and **B**) by incorporating a NAD(P)H-sensing quinolinium electron-deficient acceptor onto the coumarin framework, using vinyl and thiophene connection bridges at the 3-position (Scheme 2). Probe **A** was synthesized via a palladium-catalyzed Heck reaction involving 7-(diethylamino)-3-vinyl-2H-chromen-2-one (**3**) and 3-bromoquinoline (**4**), yielding (E)-7-(diethylamino)-3-(2-(quinolin-3-yl)vinyl)-2H-chromen-2-one (**5**), which was subsequently methylated. Probe **B** was synthesized via a multistep process, beginning with a palladium-catalyzed Suzuki coupling reaction between quinolin-3-ylboronic (**6**) acid and 2,5-dibromothiophene (**7**), yielding 3-(5-bromothiophen-2-yl)quinoline (**8**). Subsequently, compound **8** underwent a palladium-catalyzed Heck coupling reaction between 7-(diethylamino)-3-vinyl-2H-chromen-2-one (**3**) and 3-(5-bromothiophen-2-yl)quinoline (**8**), yielding (E)-7-(diethylamino)-3-(2-(5-(quinolin-3-yl)thiophen-2-yl)vinyl)-2H-chromen-2-one (**9**), followed by methylation of compound **9** (Scheme 2). To heighten the electron-deficient characteristic of the probe, thereby expediting its reduction by NAD(P)H, we constructed probe **C** by replacing the lactone carbonyl group in compound **5** with a dicyano group, resulting in the synthesis of (E)-2-(7-(diethylamino)-3-(2-(quinolin-3-yl)vinyl)-2H-chromen-2-ylidene)malononitrile (**11**), and subsequently methylating compound **11** (Scheme 2).

3.2. Optical Responses of the Probes to NADH. The optical behavior of the three probes upon exposure to NADH was investigated. Probe **A** exhibits a weak absorption at 304, a midsized one at 461 nm, and a faint fluorescence peak at 537 nm under 460 nm excitation in the absence of NADH. This subdued fluorescence emanates from the quenching effect induced by the partial deactivation of ICT within a D−π−A−π−A configuration, comprising two electron-withdrawing acceptors and one electron-rich donor (Scheme 1). Upon incremental addition of NADH to the probe solution, we observed the expected increase in the absorption due to added NADH at 340 nm[54] and a decrease and slight shift in the absorbance at 461−452 nm due to the reaction of probe **A** with NADH to form **AH**. There are substantial increases in the intensity and a red shift in position from 537 to 561 nm in the

https://doi.org/10.1021/acsabm.4c00595
ACS Appl. Bio Mater. 2024, 7, 5437−5451

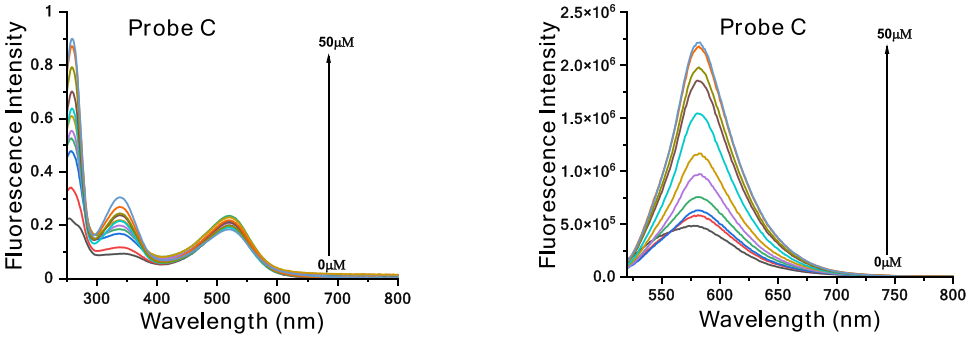

Figure 3. Absorption and fluorescence spectra of 10 μM probe **C** (521 nm) in the absence and presence of different NADH concentrations in pH 7.4 phosphate buffers under an excitation of 500 nm.

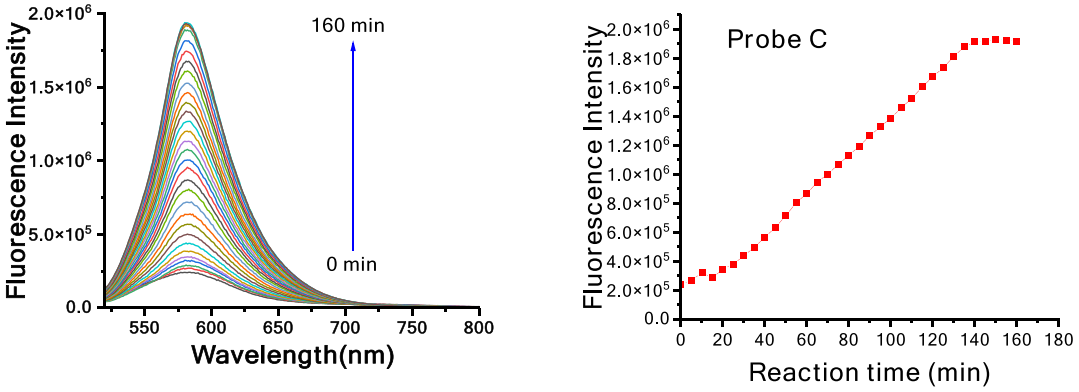

Figure 4. Fluorescence spectra and corresponding fluorescence intensities at 580 nm of a 10 μM concentration of probe **C** when subjected to varying reaction times in the presence of 50 μM NADH.

fluorescence after the addition of NADH with a linear response to 200 μM, and the limit of detection was calculated to 0.01 μM (Figure S22). These fluorescence enhancements stem from the reduction of the electron-withdrawing quinolinium acceptor by NADH to the electron-donating 1-methyl-1,4-dihydroquinoline donor, thereby augmenting ICT within a D−π−A−π−D system, where two electron-rich donors transfer electrons to the electron-withdrawing acceptor (Figure 1). Probe **A** exhibits fluorescence responsiveness to NADH within 200 min, attributed to the reduction in charge density of the 3-quinolinium acceptor via π-conjugation with the coumarin dye, thereby slowing down the reduction of 3-quinolinium within the probe by NADH (Figure S20). Our previously established methodology utilized a thiophene connection bridge to effectively modulate cyanine dyes toward the near-infrared spectrum for NAD(P)H sensing applications.[20] This strategy was employed in the synthesis of probe **B**, utilizing thiophene to link coumarin with an electron-withdrawing quinolinium acceptor, again for NAD(P)H sensing purposes. Probe **B** displays a weak absorption at 465 nm (Figure 2). Unexpectedly, despite the incorporation of the coumarin connection bridge, probe **B** failed to exhibit longer emission wavelengths, instead demonstrating turn-on fluorescence responses to NADH at 535 nm with a linear response to 50 μM, and the limit of detection was calculated and found to be 0.06 μM (Figure S23). Furthermore, probe **B** demonstrated a pronounced fluorescence background even in the absence of NADH (Figure 2), with its fluorescence responsiveness to NADH registering at 160 min (Figure S21).

To facilitate the rapid reduction of the probe by NADH, we synthesized probe **C** by substituting the lactone carbonyl group of probe **A** with a dicyano moiety, thereby augmenting the reaction kinetics with NADH. Probe **C** displays a similar absorption pattern to probe **B** exhibits a prominent absorption peak at 521 nm and a faint fluorescence peak at 574 nm in the absence of NADH (Figure 3). Upon introducing NADH to the solution of probe **C**, there is a marginal increase in absorbance at 521 nm and substantial enhancements in fluorescence at 583 nm, accompanied by a slight red shift with a linear response to 50 μM, and the calculated limit of detection was found to be 0.01 μM (Figure S24). The incorporation of an electron-deficient functionality within probe **C**, achieved by replacing the lactone carbonyl group of probe **A** with a dicyano group, facilitates the tuning of coumarin to emit longer wavelengths and accelerates the fluorescence response to NADH compared to probe **A**. Notably, probe **C** demonstrates consistent fluorescence responses to NADH within 140 min (see Figure 4).

3.3. Theoretical Results. Theoretical calculations were conducted to examine the geometry and electronic absorption properties of the probes. Probe **A** contains a planar arrangement between the quinolinium and coumarin moieties (Figure S31). However, in probe **AH** (Figure S34), the quinolinium group with the added hydride twists slightly as a result of an adjacent H atom situated in between this CH_2 entity and also the loss of planarity in this quinolinium moiety resulting in an interplanar angle of 40° to the coumarin section. In probe **B** (Figure S37), the coumarin and the vinyl thiophene groups are in the same plane with the plane of the quinoline moiety twisted and at an angle of 26° to that plane. In contrast, these groups are in the same plane in probe **BH** (Figure S40). The dicyano group in probe **C** results in deviations away from

https://doi.org/10.1021/acsabm.4c00595
ACS Appl. Bio Mater. 2024, 7, 5437−5451

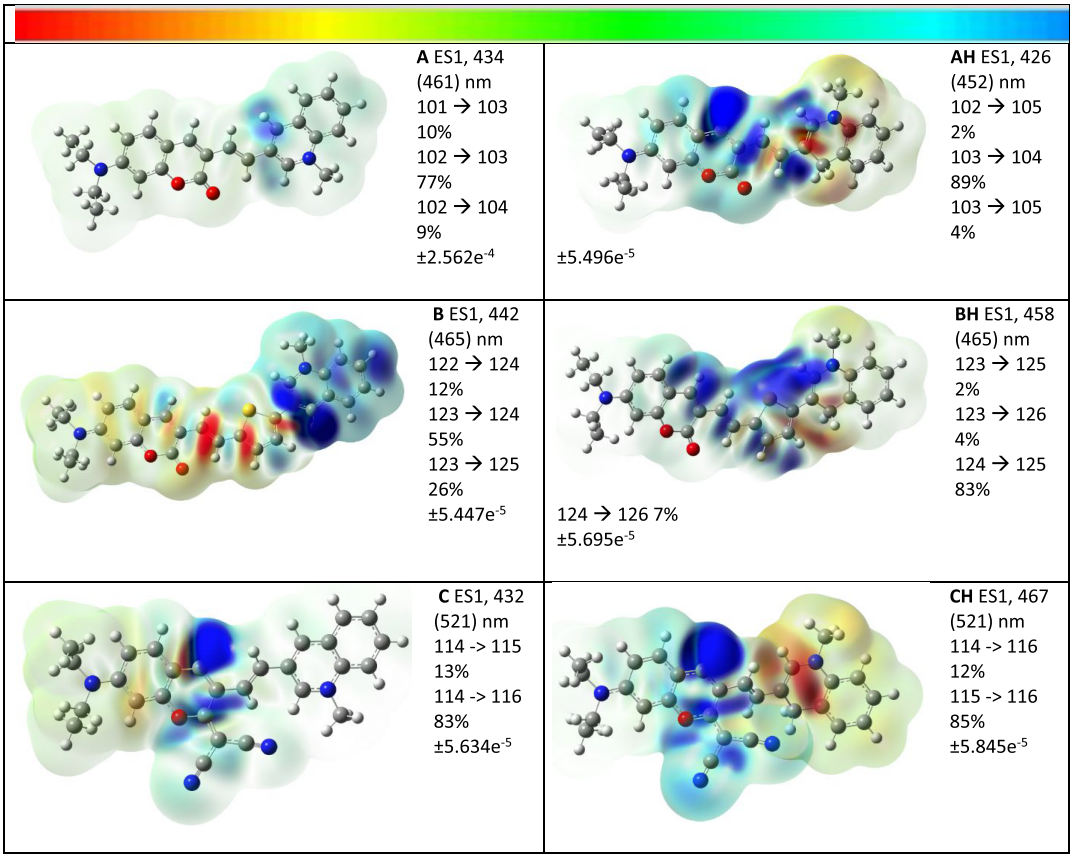

Figure 5. Variations in current density through isosurfaces representing probes **A**, **AH**, **B**, **BH**, **C**, and **CH** and a detailed breakdown of energized states (ES) quantities, including both theoretical and experimental wavelengths, LCAO transitions, and their proportional contribution percentages. The figure also includes a key explaining each color gradation with the scale on the top of the figure. Diagrams related to the numerically labeled LCAOs can be found in the supplementary data for further clarification.

planarity in the middle vinyl group. This deviation results from the minimization of steric hindrance between the dicyano group attached to coumarin and the proximal H atom on the vinyl group and is evident in both probe **C** (Figure S43) and **CH** (Figure S46).

The results of TD-DFT calculations and electron current density transitions are displayed in Figure 5. There is reasonable agreement with the theoretical and experimental absorption values with differences ranging from 7 nm in probe **BH** to 27 nm for probe **A**. Probe **C** (89 nm) and **CH** (54 nm) contain larger differences, probably because the optimized geometry was not planar around the vinyl moiety. As is evident in Figure 5, in probes **A** and **B**, the electronic transition originates from the coumarin side of the molecule and ends up on the quinoline moieties. For **AH** and **BH**, the transition shifts and originates from the site of hydride addition, i.e., the quinoline moiety, and ends up in the middle vinyl section. With probes **C** and **CH**, the electronic transition originates from different ends as with probes **A** and **B**, but the transition ends up in both cases on the dicyano-substituted coumarin section due to its superior electron stabilizing capability.

The images in Figure 5 for probes **A**, **B**, and **C** also illustrate a possible reason for the order of reactivity with the hydride addition. With these probes, **C** was found to react the fastest with hydride addition complete after 140 min. An examination of the magnitude of the Mulliken charge on the C atom (trans to the N-Me group) which binds the hydrogen would reveal that **A** is at 0.458, **B** at 0.108, and **C** is at 0.165. As the C atom on probe **A** is the most positive, one would expect that this would react at the fastest rate; however, kinetic factors may be at work here. The illustrations in Figure 5 suggest that there is much less overall electron density in probe **C** compared to the others, possibly because it is out of the quinolinium plane as described above. This may make the reaction with NADH more likely resulting in a shorter reaction time.

3.4. Probe Selectivity, Photostability, and Cytotoxicity Study. Probe **C** exhibits remarkable specificity toward NAD(P)H when compared to a wide array of other substances, spanning cations such as Co^{2+}, Al^{3+}, Sn^{2+}, Cu^{2+}, Ca^{2+}, Mo^{2+}, Fe^{3+}, and Sn^{2+}, anions like HCO_3^-, HSO_3^-, SO_4^{2-}, CN^-, PO_4^{3-}, NO_3^-, Cl^-, including biomolecules such as glutathione and cysteine, amino acids including DL-tyrosine, methionine, and lysine, and carbohydrates like glucose, ribose, fructose, lactate, galactose, and pyruvate (Figure S28). This elevated level of specificity is important for the precise identification and measurement of NAD(P)H, a vital coenzyme pivotal in energy metabolism and numerous cellular functions.

The resilience to photobleaching or loss of fluorescence over extended light exposure, known as photostability, is a crucial attribute for fluorophores. Probes **A**, **B**, and **C** showcase notable photostability, evident in their minimal fluorescence alterations following 2 h of excitation at 500 nm (Figures S25–S27). Such durability is required for endeavors necessitating prolonged or recurrent imaging, as photobleaching can undermine signal integrity and image fidelity over time.

https://doi.org/10.1021/acsabm.4c00595
ACS Appl. Bio Mater. 2024, 7, 5437−5451

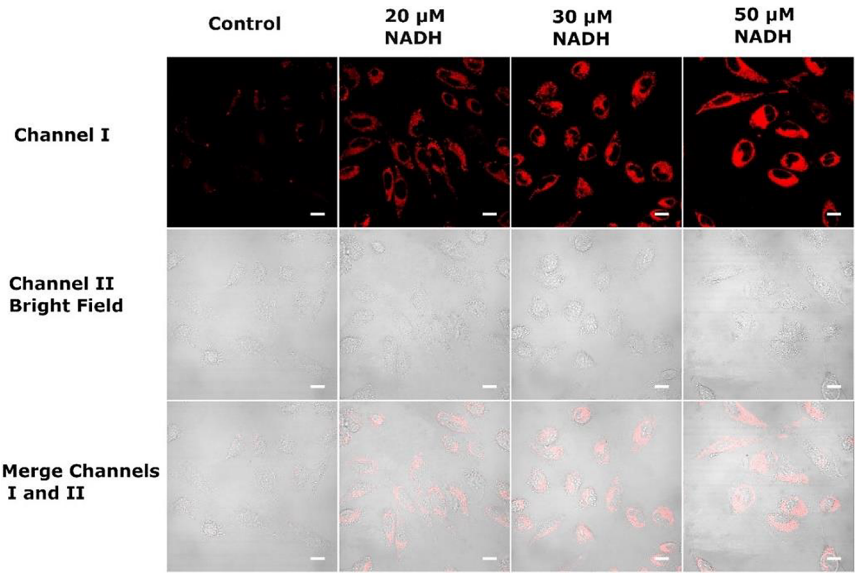

Figure 6. Confocal laser fluorescence microscopy images illustrating the impact of varying NADH concentrations (0 μM as control, 20, 30, and 50 μM) on HeLa cells for 30 min, followed by a 30 min incubation with 5 μM probe **C**. Fluorescent signals were captured within the 550−650 nm range using a 488 nm excitation wavelength. Scale bars represent 50 μm.

To evaluate the toxicity of probe **C**, we employed an MTT assay following established procedures[32,34,55−61] HeLa cells were exposed to probe **C**, and we measured the change in the yellow MTT dye to a purple formazan product due to enzymatic reduction within mitochondria, indicating cell viability. Our findings demonstrate that cell viability remains above 83% at a concentration of 50 μM (see Figure S30), suggesting that the probe does not induce toxicity in the cells. The utilization of this probe with minimal cytotoxicity is essential as it minimizes adverse effects on cell behavior, ensuring more accurate experimental results. Furthermore, low cytotoxicity facilitates prolonged exposure durations or repeated measurements, which are vital for longitudinal studies or monitoring treatment responses.

3.5. Visualizing Dynamic Cellular NAD(P)H Fluctuations across Various Chemical Treatments. Due to its longer wavelength emission and rapid responsiveness to NAD(P)H, probe **C** was selected for monitoring dynamic cellular NAD(P)H levels across various chemical treatments. In order to verify the specificity of probe **C** toward intracellular NAD(P)H levels, control experiments and NADH dose−response experiments were conducted using HeLa cells. In the control experiment, HeLa cells were subjected to 5 μM probe **C** in glucose-free DMEM medium for 30 min without prior exposure to NADH. Fluorescence imaging demonstrated minor fluorescence at this stage (Figure 6), indicating a low basal level of intrinsic NAD(P)H. This indicates that probe **C** remains inactive if NADH levels are not elevated. Conversely, HeLa cells, pretreated with different concentrations of NADH (20, 30, and 50 μM) for 30 min in glucose-free DMEM, displayed an increase in fluorescence dependent on dose upon subsequent incubation with probe **C** (Figure 6). Higher concentrations of NADH pretreatment resulted in higher fluorescence intensity, directly proportional to the extracellular NADH levels. This dose-dependent response affirms the specificity of probe **C** in detecting differences in intracellular NADH, with increased fluorescence indicating elevated NADH content. The results from both control and dose−response studies validate the capability of probe **C** to selectively monitor dynamic alterations in NADH levels without nonspecific activation. The strong correlation observed between NADH levels and probe **C** fluorescence allows for reliable quantitative imaging.

We hypothesized that the single positive charge on probe **C** could facilitate targeting of mitochondria via opposite charge interactions with the negative mitochondrial membrane potential. To evaluate this hypothesis, we conducted colocalization experiments in HeLa cells utilizing the mitochondrial-specific cyanine dye (IR-780). Preceding this, cells were exposed to 20 μM NADH in glucose-free DMEM for 30 min, followed by simultaneous exposure to 5 μM probe **C** and 5 μM cyanine dye (IR-780) for another 30 min. Analysis using the Pearson correlation coefficient demonstrated a strong colocalization between probe **C** and cyanine dye, with a coefficient value of 0.915 (Figure 7). This robust correlation

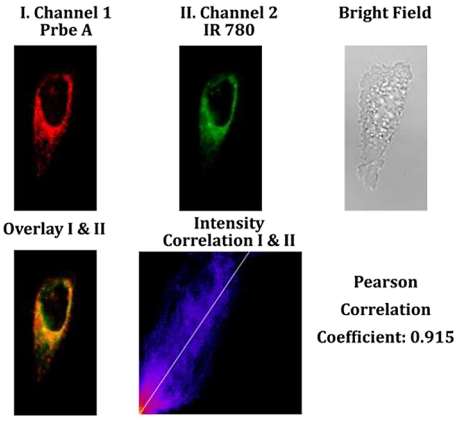

Figure 7. Confocal laser fluorescence microscopy images demonstrating the effects of varying concentrations of NADH (20 μM) on HeLa cells following a 30 min exposure period, followed by coincubation with 5 μM of probe **C** and 5 μM of cyanine dye (IR-780) for an additional 30 min. Fluorescent signals were captured within the range of 550−650 nm using a 488 nm excitation wavelength. Scale bars indicate 50 μm.

https://doi.org/10.1021/acsabm.4c00595
ACS Appl. Bio Mater. 2024, 7, 5437−5451

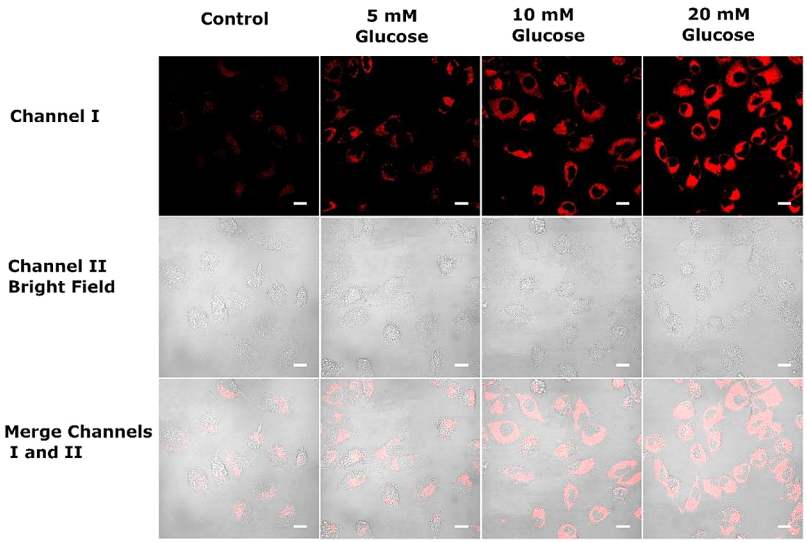

Figure 8. Confocal laser fluorescence microscopy images illustrating the response of HeLa cells to different glucose concentrations (0 mM as control, 5, 10, and 20 mM) after a 30 min exposure, followed by incubation with probe **C** (5 μM) for an additional 30 min. Imaging was performed within the 550−650 nm range with a 488 nm excitation wavelength. Scale bar = 50 μm.

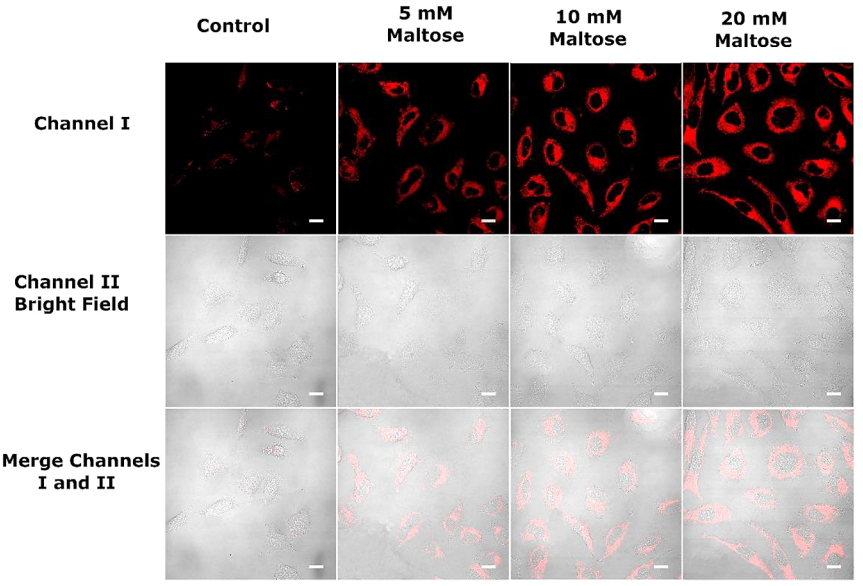

Figure 9. Confocal laser fluorescence microscopy images displaying HeLa cells subjected to different maltose concentrations (0 mM as control, 5, 10, and 20 mM) for 30 min, followed by incubation with probe **C** (5 μM) for an additional 30 min. Imaging was performed within the 550−650 nm range using a 488 nm excitation wavelength. Scale bars indicate 50 μm.

supports our assertion that the cationic nature of probe **C** facilitates selective staining of mitochondria, resulting in accumulation within the negatively charged mitochondria. The ability to detect NADH levels within mitochondria holds significant importance, given their pivotal role as cellular powerhouses reliant on NADH as an indispensable electron carrier for oxidative phosphorylation and ATP synthesis.

One of our primary objectives was to investigate the impact of varying glucose availability on intracellular NADH levels. Glucose plays a pivotal role in NADH generation via glycolysis, wherein it undergoes conversion to pyruvate, leading to NADH production within the cell's cytosol. We posited that augmenting extracellular glucose levels would bolster glycolysis, consequently elevating NADH production. To verify this hypothesis, we conducted an experiment utilizing HeLa cells, subjecting them to varied glucose concentrations (0, 5, 10, and 20 mM) in glucose-free DMEM for 30 min, followed by treatment with 5 μM probe **C** in glucose-free DMEM for another 30 min. Subsequently, fluorescence imaging was conducted employing an excitation wavelength of 488 nm and observing emission ranging from 550 to 650 nm. As anticipated, heightened glucose concentrations elicited a progressive rise in fluorescence intensity, indicative of increased NADH levels (Figure 8). The absence of glucose yielded minimal baseline fluorescence, denoting low NADH levels. Nonetheless, fluorescence levels exhibited a dose-dependent escalation with 5, 10, and 20 mM glucose treatments, signifying that elevated extracellular glucose levels spurred glycolysis and NADH generation.[12,13,20,23,24] These observations underscore the profound influence of glucose levels on glycolytic activity and NADH production. This methodology presents a valuable avenue for delving into redox

https://doi.org/10.1021/acsabm.4c00595
ACS Appl. Bio Mater. 2024, 7, 5437−5451

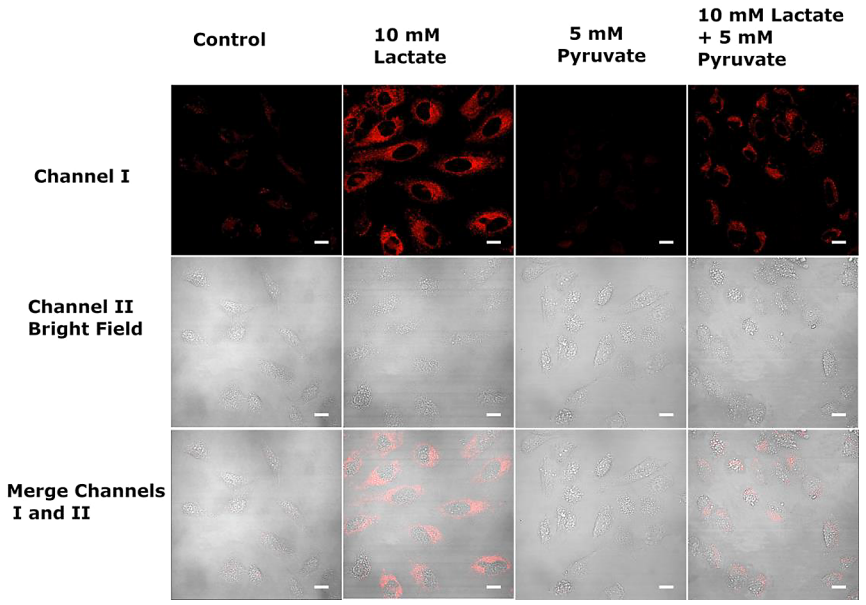

Figure 10. Fluorescence emission images depicting the response of HeLa cells under various pretreatment conditions, including lactate, pyruvate, or a combination of both, in a glucose-deficient DMEM medium, observed over 30 min. Subsequently, the cells were coincubated with 5 μM of probe **C** in glucose-deficient DMEM medium for an additional 30 min. Fluorescence emissions were captured using excitation at 488 nm and detecting emissions ranging from 550 to 650 nm.

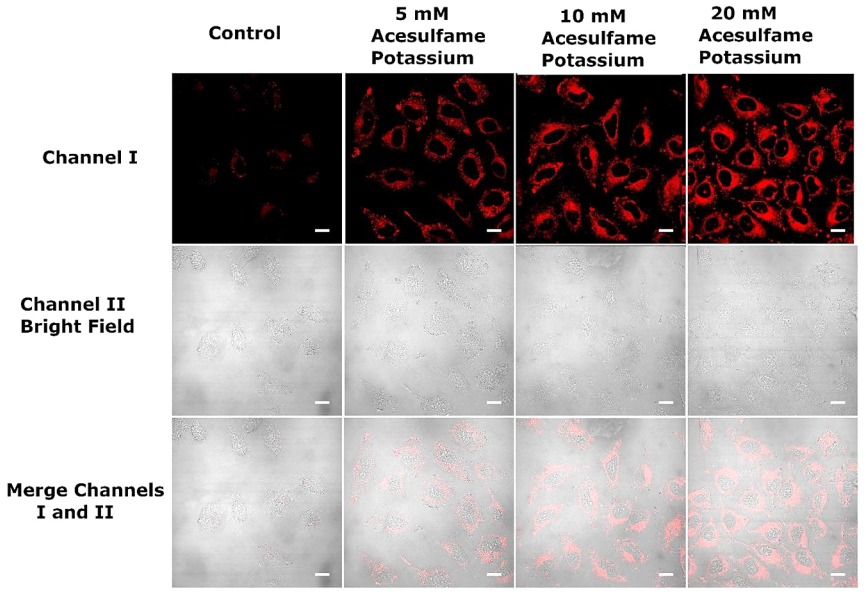

Figure 11. Confocal laser fluorescence microscopy images illustrating the impact of different concentrations of Ace-K (0 mM as control, 5, 10, and 20 mM) on HeLa cells after a 30 min exposure, followed by a subsequent 30 min incubation with 5 μM probe **C**. Fluorescence signals were captured between 550 and 650 nm using a 488 nm excitation wavelength. The scale bar represents 50 μm, indicating the spatial dimensions of the images.

biology and the intricacies of cellular metabolism within its natural milieu.

Maltose, a disaccharide formed from two glucose molecules bonded by an $\alpha(1 \rightarrow 4)$ glycosidic bond, is commonly utilized in brewing beer, baking, and the food industry as a sweetener and fermentation substrate.[62] Although less sweet than glucose or sucrose, maltose can be broken down into glucose, serving as an energy source for organisms.[62] Our investigation focused on the impact of maltose on NAD(P)H levels in HeLa cells through pretreatment with varying concentrations of maltose followed by incubation with probe **C**. Results revealed a significant increase in cellular fluorescence upon maltose treatment compared to an equivalent concentration of glucose, implying a more pronounced elevation in NAD(H) levels with maltose (Figure 9). This suggests efficient enzymatic breakdown of maltose into glucose within cells.[62] Notably, fluorescence levels demonstrated a dose-dependent increase with maltose treatments of 5, 10, and 20 mM, implying that elevated extracellular glucose levels stimulate glycolysis and NADH generation.

The impact of exogenous pyruvate and lactate on glycolytic flux and intracellular NADH levels was also explored.[63] In cancer cells, pyruvate is primarily converted to lactate during aerobic glycolysis, leading to NADH consumption.[63] We

https://doi.org/10.1021/acsabm.4c00595
ACS Appl. Bio Mater. 2024, 7, 5437−5451

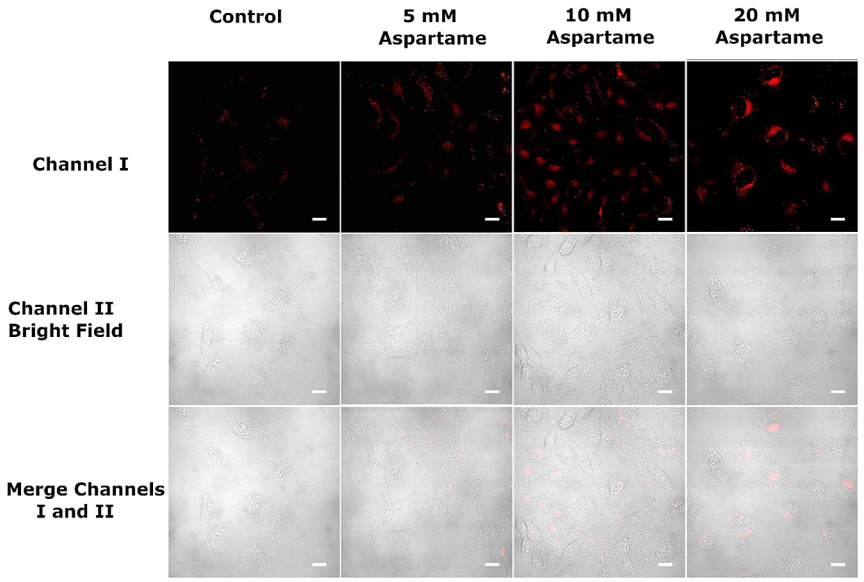

Figure 12. Confocal laser fluorescence microscopy images illustrating the impact of different concentrations of aspartame (0 mM as control, 5, 10, and 20 mM) on HeLa cells following a 30 min treatment, followed by incubation with probe **C** (5 μM) for an additional 30 min. Fluorescent imaging was performed within the 550−650 nm range using a 488 nm excitation wavelength. Scale bars represent 50 μm.

theorized that pyruvate and lactate would result in different responses on cytosolic NADH levels, which could be monitored dynamically with probe **C**. To examine this hypothesis, HeLa cells were pretreated with varied amounts of pyruvate or lactate before exposure to probe **C** (Figure 10). Interestingly, pretreatment with 5 mM pyruvate resulted in a significant reduction in fluorescence of probe **C** referenced to control cells. This suggests rapid NADH reaction by lactate dehydrogenase during the conversion of pyruvate to lactate. Furthermore, pretreatment with 10 mM lactate led to a notable increase in the fluorescence of probe **C**, indicating elevated NADH levels and enhanced intracellular NADH production. Of particular interest, joint pretreatment with 10 mM lactate and 5 mM pyruvate resulted in even higher fluorescence of probe **C** than observed in control cells. This demonstrates a synergistic effect and underscores the complex interplay between lactate and pyruvate in adjusting glycolytic NADH levels. These findings emphasize the significance of the lactate/pyruvate ratio in determining the cytosolic NADH redox state. Overall, real-time NADH imaging facilitated by probe **C** offers valuable insights into the reciprocal relationship between glycolytic substrates and NADH generation/consumption. Our research underscores the importance of comprehending these metabolic processes in cancer and other diseases, as dysregulated NADH signaling is implicated in various pathological conditions.[63,64]

Acesulfame potassium, commonly referred to as Acesulfame K or Ace-K, is an artificial sweetener known for its intense sweetness, approximately 200 times sweeter than sucrose (table sugar).[64] Widely utilized as a sugar substitute across various food and beverage categories, including soft drinks, candies, chewing gum, desserts, and dairy products, it gained approval by the Food and Drug Administration (FDA) in the United States in 1988, following its discovery in 1967.[65,66] The role of Ace-K in cellular metabolism was also explored using probe **C** in a study involving HeLa cells. Treating HeLa cells with varying concentrations of Ace-K and subsequent incubation with probe **C** revealed a significant increase in cellular fluorescence, indicative of elevated NAD(P)H levels in response to Ace-K treatment (Figure 11). This observed rise in NAD(P)H levels within HeLa cells, despite the absence of glucose in the cell culture media, is likely attributable to several interconnected mechanisms. These mechanisms encompass potential stimulation of alternative metabolic pathways, leading to enhanced NAD(P)H production; activation of NAD(P)H-producing enzymes within the tricarboxylic acid (TCA) cycle;[67] induction of cellular stress responses prompting compensatory upregulation of NAD(P)H synthesis pathways to uphold redox balance; and potential modulation of intracellular signaling cascades such as AMP-activated protein kinase (AMPK) pathways.[68] Collectively, these findings may underscore the intricate interplay between cellular metabolism, stress response, and signaling pathways in response to Ace-K exposure.

Aspartame, a widely used artificial sweetener in various foods and drinks, consists of aspartic acid bonded to methyl *L*-phenylalanine.[69,70] Our investigation using probe **C** on HeLa cells revealed that after treatment with varying aspartame concentrations and subsequent incubation with probe **C**, cellular fluorescence notably increased, indicating a significant rise in NAD(P)H levels due to aspartame treatment (Figure 12). The components of aspartame, phenylalanine, and aspartic acid can be metabolized within cells to generate energy via alternative metabolic pathways, potentially contributing to the production of NAD(P)H. Furthermore, aspartame metabolism might indirectly influence NAD(P)H levels by modulating enzyme activity involved in NAD(P)H metabolism, particularly those engaged in amino acid breakdown or redox reactions. These enzymatic activities could be altered by aspartame presence, thereby affecting NAD(P)H balance within the cell.[71] Although further research is essential to fully understand these mechanisms, these pathways suggest that aspartame could impact NAD(P)H levels in HeLa cells, even without glucose in the cell culture media. This understanding could shed light on cancer cell metabolic adaptations and responses to external factors like artificial sweeteners such as aspartame.[71]

https://doi.org/10.1021/acsabm.4c00595
ACS Appl. Bio Mater. 2024, 7, 5437−5451

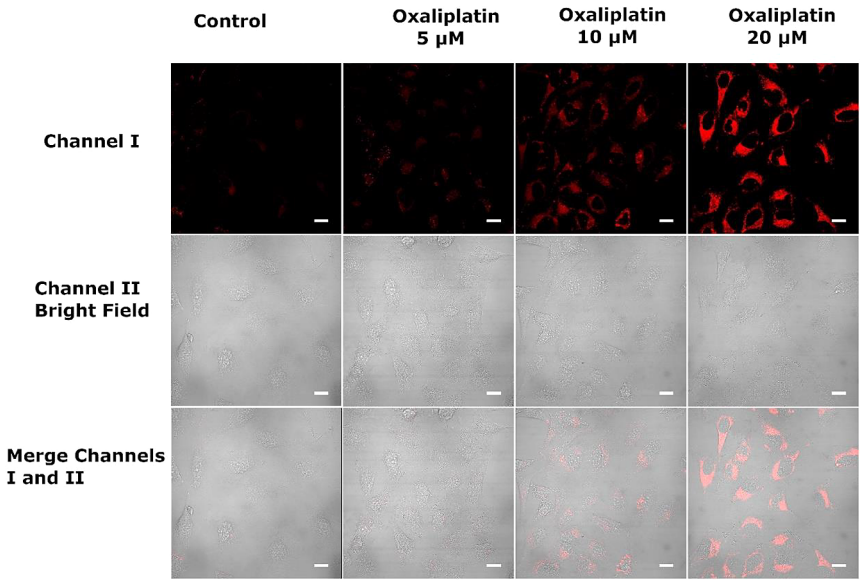

Figure 13. Confocal laser fluorescence microscopy images illustrating the response of HeLa cells to varying concentrations of oxaliplatin (0 μM as control, 5, 10, and 20 μM) for 30 min, followed by incubation with probe **C** (5 μM) for an additional 30 min. Fluorescent imaging was carried out within the 550−650 nm range using a 488 nm excitation wavelength. The scale bar denotes 50 μm.

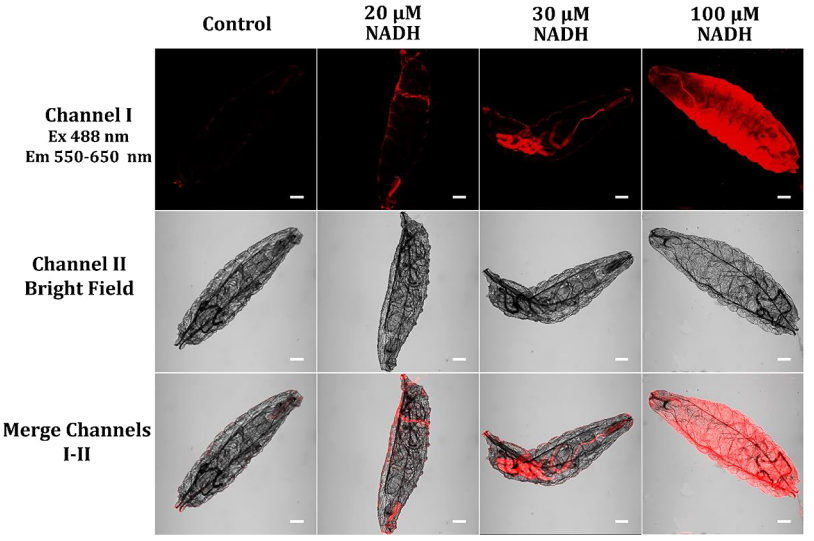

Figure 14. Fluorescence images depicting starved fruit fly larvae subjected to varying concentrations of NADH (ranging from 0 to 100 μM) for 1 h in pH 7.4 PBS buffer, followed by immersion in a PBS buffer solution containing 5 μM probe **C** for an additional 2 h. Fluorescence signals were captured within the 550−650 nm range using a 488 nm excitation wavelength. The scale bar denotes 50 μm.

Oxaliplatin, a vital chemotherapy agent utilized in combating various cancers, particularly colorectal cancer, belongs to the platinum-based class of drugs.[72−74] Its mode of action inhibits the DNA synthesis process within cells, ultimately leading to their demise.[72−74] Often integrated into treatment protocols alongside other chemotherapy drugs, oxaliplatin is administered intravenously, though not without negative ramifications such as nausea, vomiting, fatigue, and nerve damage, requiring vigilant monitoring by healthcare providers.[72−74] In our investigation, we employed probe **C** to examine oxaliplatin's impact on NAD(P)H levels within HeLa cells (Figure 13). Post-treatment with oxaliplatin and subsequent incubation with probe **C**, results in a significant surge in cellular fluorescence, presumably due to a marked elevation in NAD(P)H levels following oxaliplatin exposure. One plausible mechanism driving this increase in NAD(P)H levels involves oxaliplatin's interference with DNA synthesis.[72−74] The formation of platinum-DNA adducts by oxaliplatin initiates DNA damage, preventing cellular repair and copying mechanisms that heavily rely on NAD(P)H as a cofactor for various enzymes essential in DNA repair and copying pathways.[72−74] Consequently, the reduced demand for NAD(P)H to sustain these repair processes in oxaliplatin-treated cells contributes to the observed elevation in cellular NAD(P)H levels. Moreover, oxaliplatin-induced cellular stress and damage can trigger metabolic shifts within cells, encompassing alterations in glycolysis, the citric acid cycle, and oxidative phosphorylation. These metabolic adjustments can perturb the balance of NAD+ and NADH (or NADP+ and NADPH) within cells, leading to an increase in NAD(P)H levels. Furthermore, oxaliplatin treatment may alter the function of enzymes involved in NAD(P)H metabolism, such as

https://doi.org/10.1021/acsabm.4c00595
ACS Appl. Bio Mater. 2024, 7, 5437−5451

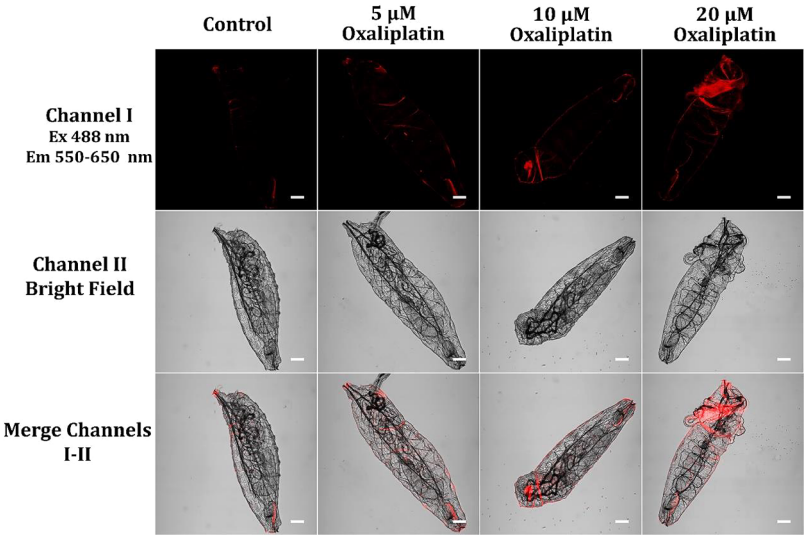

Figure 15. Fluorescence microscopy images illustrating starved fruit fly larvae treated with different concentrations of oxaliplatin (ranging from 0 to 20 μM) for 1 h in pH 7.4 PBS buffer, followed by immersion in a PBS buffer solution containing 5 μM probe **C** for an additional 2 h. Fluorescence signals were captured within the 550−650 nm range using a 488 nm excitation wavelength. The scale bar denotes 50 μm.

nicotinamide phosphoribosyltransferase (NAMPT), a pivotal component for the regenerative pathway of NAD+ biosynthesis.[75] Modulations in the activity of such enzymes can impact cellular NAD(P)H levels. In summary, the escalation in NAD(P)H levels within HeLa cells following oxaliplatin treatment may arise from a complex interplay of cellular responses, including inhibited DNA damage repair, metabolic reprogramming, and alterations in enzyme activities associated with NAD(P)H metabolism.[75] This multifaceted response may underscore the intricate mechanisms underlying oxaliplatin's therapeutic effects and provide valuable insights into its mode of action at the cellular level.

We employed freshly starved-hatched fruit fly larvae as a model system to assess the efficacy of probe **C** in monitoring NAD(P)H dynamics in vivo.[13,55] The selection of these larvae was due to their reduced NAD(P)H levels, a result of metabolic adjustments in response to lacking nutrients upon hatching.[13,55] In the absence of food, larval metabolism consumes NAD(P)H, a crucial coenzyme central to cellular reactions. This consumption establishes a controlled baseline, optimal for scrutinizing NAD(P)H fluctuations in response to various treatments.[13,55] In our investigations, control larvae treated with probe **C** in PBS exhibited minimal fluorescence, indicating consumption of NAD(P)H (Figure 14). Upon exposure to different concentrations of NADH, we observed a dose-dependent rise in fluorescence, mirroring the increase in NAD(P)H levels (Figure 14). This illustrates the sensitivity of probe **C** in real-time monitoring of NAD(P)H changes in reaction to NADH. Similarly, exposure to oxaliplatin resulted in an enhancement of fluorescence due to the formation of porbe **CH**, compared to the control group, indicating heightened NAD(P)H levels induced by oxaliplatin-induced stress (Figure 15). This elevation in NAD(P)H likely arises from metabolic adjustments and cellular stress response pathways triggered by oxaliplatin toxicity. Our observations from experiments with starvation-hatched larvae highlight the effectiveness of probe **C** in elucidating NAD(P)H dynamics influenced by external compounds within living organisms. The findings concerning NADH and oxaliplatin shed light on larval metabolism and cellular stress responses. Importantly, they affirm the utility of probe **C** for studying NAD(P)H signaling pathways in biomedical research contexts. Our study offers insight into NAD(P)H dynamics in living organisms, facilitated by probe **C**, and underscores its significance in advancing biomedical research aimed at unraveling intricate cellular processes and responses to external stimuli.

4. CONCLUSIONS

In summary, our study presents a comprehensive investigation into the development and characterization of three novel fluorescent probes **A**, **B**, and **C**, designed for continuous tracking of NAD(P)H levels in live cells. The incorporation of coumarin platforms and electron-deficient functionalities resulted in the formation of probe **C** which demonstrated rapid responsiveness and selective targeting of mitochondria. The specificity of probe **C** toward intracellular NAD(P)H levels was validated through control experiments and dose−response studies in HeLa cells, offering a reliable tool for quantitative imaging of NAD(P)H dynamics. Furthermore, our exploration into the impact of metabolic substrates and chemotherapeutic agents on cellular NAD(P)H levels provided evidence of complex interactions underlying cellular metabolism, stress responses, and disease mechanisms. From the influence of glucose availability to the responses to artificial sweeteners and chemotherapy drugs, our findings provide valuable insights into cellular adaptations and responses to external stimuli. Importantly, our in vivo studies using starved fruit fly larvae highlight the applicability of probe **C** in monitoring NAD(P)H dynamics in living organisms, emphasizing its utility in biomedical research. The versatility and reliability of probe **C** underscore its significance as a valuable tool for probing NAD(P)H signaling pathways, advancing our understanding of cellular metabolism, redox biology, and disease pathogenesis. Future research utilizing probe **C** holds promise for unraveling intricate cellular processes and suggesting targeted therapeutic interventions.

https://doi.org/10.1021/acsabm.4c00595
ACS Appl. Bio Mater. 2024, 7, 5437−5451

■ ASSOCIATED CONTENT

Supporting Information

The Supporting Information is available free of charge at https://pubs.acs.org/doi/10.1021/acsabm.4c00595.

Instrumentation, reagents, and synthetic approach; NMR and MS spectra of the intermediates and probes; MS spectra of the reaction products of the probes with NADH; time-dependent fluorescence measurement of probes A and B; linear fluorescence responses of probes to NADH; photostability of the probes; probe selectivity; cell culture; drug treatment of HeLa cells; D. melanogaster larval imaging; assessing cell viability using MTT assay; and theoretical calculations (PDF)

■ AUTHOR INFORMATION

Corresponding Authors

Sushil K. Dwivedi − *Department of Chemistry, Michigan Technological University, Houghton, Michigan 49931, United States*; Email: sdwive2@mtu.edu

Rudy L. Luck − *Department of Chemistry, Michigan Technological University, Houghton, Michigan 49931, United States*; orcid.org/0000-0001-5436-1942; Email: rluck@mtu.edu

Haiying Liu − *Department of Chemistry, Michigan Technological University, Houghton, Michigan 49931, United States*; orcid.org/0000-0001-8351-2017; Email: hyliu@mtu.edu

Authors

Adenike Mary Olowolagba − *Department of Chemistry, Michigan Technological University, Houghton, Michigan 49931, United States*

Micah Olamide Idowu − *Department of Chemistry, Michigan Technological University, Houghton, Michigan 49931, United States*

Dilka Liyana Arachchige − *Department of Chemistry, Michigan Technological University, Houghton, Michigan 49931, United States*

Omowunmi Rebecca Aworinde − *Department of Chemistry, Michigan Technological University, Houghton, Michigan 49931, United States*

Olivya Rose Graham − *Department of Biological Science, Michigan Technological University, Houghton, Michigan 49931, United States*

Thomas Werner − *Department of Biological Science, Michigan Technological University, Houghton, Michigan 49931, United States*

Complete contact information is available at: https://pubs.acs.org/10.1021/acsabm.4c00595

Notes

The authors declare no competing financial interest.

■ ACKNOWLEDGMENTS

The research investigation received sponsorship from the National Institute of General Medical Sciences, National Institutes of Health, under the auspices of Award Numbers 2R15GM114751 and R15GM114751 for H.L., as well as R15 GM146206-01 for both H.L. and R.L.L. Grateful acknowledgment is extended to the National Science Foundation for their financial backing via award number 2117318. This funding facilitated the acquisition of a new NMR spectrometer for the characterization of chemical structures of the fluorescent probes, with H.L. being one of the grant recipients. Computational calculations for the fluorescent probes were conducted utilizing a high-performance computing infrastructure situated at Michigan Technological University. The invaluable support provided by these entities is deeply appreciated, as it has been instrumental in advancing this research endeavor.

■ REFERENCES

(1) Rehman, A. U.; Anwer, A. G.; Gosnell, M. E.; Mahbub, S. B.; Liu, G.; Goldys, E. M. Fluorescence quenching of free and bound NADH in HeLa cells determined by hyperspectral imaging and unmixing of cell autofluorescence. *Biomed. Opt. Express* **2017**, *8* (3), 1488−1498.

(2) Berthiaume, J. M.; Kurdys, J. G.; Muntean, D. M.; Rosca, M. G. Mitochondrial NAD+ NADH Redox State and Diabetic Cardiomyopathy. *Antioxidants & Redox Signaling* **2019**, *30* (3), 375−398.

(3) Willems, P.; Smeitink, J. A. M.; Koopman, W. J. H. Mitochondrial dynamics in human NADH:ubiquinone oxidoreductase deficiency. *Int. J. Biochem. Cell Biol.* **2009**, *41* (10), 1773−1782.

(4) Ying, W. H. NAD+ and NADH in cellular functions and cell death. *Frontiers in Bioscience-Landmark* **2006**, *11*, 3129−3148.

(5) Sarniak, A.; Lipinska, J.; Tytman, K.; Lipinska, S. Endogenous mechanisms of reactive oxygen species (ROS) generation. *Postepy Hig. Med. Dosw.* **2016**, *70*, 1150−1164.

(6) Curtis, W. M.; Seeds, W. A.; Mattson, M. P.; Bradshaw, P. C. NADPH and Mitochondrial Quality Control as Targets for a Circadian-Based Fasting and Exercise Therapy for the Treatment of Parkinson's Disease. *Cells* **2022**, *11* (15), 2416.

(7) Kassan, M.; Choi, S. K.; Galán, M.; Lee, Y. H.; Trebak, M.; Matrougui, K. Enhanced p22 phox expression impairs vascular function through p38 and ERK1/2 MAP kinase-dependent mechanisms in type 2 diabetic mice. *American Journal of Physiology-Heart and Circulatory Physiology* **2014**, *306* (7), H972−H980.

(8) She, J.; Sheng, R.; Qin, Z. H. Pharmacology and Potential Implications of Nicotinamide Adenine Dinucleotide Precursors. *Aging Dis.* **2021**, *12* (8), 1879−1897.

(9) Hong, S. N.; Pawel, G. T.; Pei, R. J.; Lu, Y. Recent progress in developing fluorescent probes for imaging cell metabolites. *Biomedical Materials* **2021**, *16* (4), No. 044108.

(10) Park, S. Y.; Yoon, S. A.; Cha, Y. J.; Lee, M. H. Recent advances in fluorescent probes for cellular antioxidants: Detection of NADH, hNQO1, H2S, and other redox biomolecules. *Coord. Chem. Rev.* **2021**, *428*, No. 213613.

(11) Sun, P. J.; Zhang, H. X.; Sun, Y. Q.; Liu, J. The recent development of fluorescent probes for the detection of NADH and NADPH in living cells and in vivo. *Spectrochim. Acta Part A Mol. Biomol. Spectrosc.* **2021**, *245*, No. 118919.

(12) Zhang, Y. B.; Arachchige, D. L.; Olowolagba, A.; Luck, R. L.; Liu, H. Y. Near-infrared fluorescent probe based on rhodamine derivative for detection of NADH in live cells. *Methods* **2022**, *204*, 22−28.

(13) Dwivedi, S. K.; Arachchige, D. L.; Waters, M.; Jaeger, S.; Mahmoud, M.; Olowolagba, A. M.; Tucker, D. R.; Geborkoff, M. R.; Werner, T.; Luck, R. L.; et al. Near-infrared absorption and emission probes with optimal connection bridges for live monitoring of NAD(P)H dynamics in living systems. *SENSORS AND ACTUATORS B-CHEMICAL* **2024**, *402*, No. 135073.

(14) Li, M. Z.; Liu, C.; Zhang, W. J.; Xu, L. F.; Yang, M. M.; Chen, Z. L.; Wang, X. X.; Pu, L. L.; Liu, W. L.; Zeng, X. S.; et al. An NADH-selective and sensitive fluorescence probe to evaluate living cell hypoxic stress. *J. Mater. Chem. B* **2021**, *9* (46), 9547−9552.

(15) Sharma, H.; Tan, N. K.; Trinh, N.; Yeo, J. H.; New, E. J.; Pfeffer, F. M. A fluorescent naphthalimide NADH mimic for continuous and reversible sensing of cellular redox state. *Chem. Commun.* **2020**, *56* (15), 2240−2243.

(16) Dai, F.; Zhang, S. X.; Zhou, B.; Duan, D. C.; Liu, J. R.; Zheng, Y. L.; Chen, H.; Zhang, X. Y.; Zhang, Y. Cellular and Intravital Imaging of NAD(P)H by a Red-Emitting Quinolinium-Based Fluorescent Probe that Features a Shift of Its Product from Mitochondria to the Nucleus. *Anal. Chem.* **2022**, *95* (2), 1335−1342.
(17) Joo, J. H.; Won, M.; Park, S. Y.; Park, K.; Shin, D. S.; Kim, J. S.; Lee, M. H. A dicyanocoumarin-fused quinolinium based probe for NAD(P)H and its use for detecting glycolysis and hypoxia in living cells and tumor spheroids. *Sens. Actuators B: Chem.* **2020**, *320*, No. 128360.
(18) Tian, Y.; Jiang, W. L.; Wang, W. X.; Mao, G. J.; Li, Y. F.; Li, C. Y. NAD(P)H-triggered probe for dual-modal imaging during energy metabolism and novel strategy of enhanced photothermal therapy in tumor. *Biomaterials* **2021**, *271*, No. 120736.
(19) Zhao, Y. H.; Wei, K. Y.; Kong, F. P.; Gao, X. N.; Xu, K. H.; Tang, B. Dicyanoisophorone-Based Near-Infrared-Emission Fluorescent Probe for Detecting NAD(P)H in Living Cells and in Vivo. *Anal. Chem.* **2019**, *91* (2), 1368−1374.
(20) Dwivedi, S. K.; Arachchige, D. L.; Olowolagba, A.; Mahmoud, M.; Cunnien, J.; Tucker, D. R.; Fritz, D.; Werner, T.; Luck, R. L.; Liu, H. Y. Thiophene-based organic dye with large Stokes shift and deep red emission for live cell NAD(P)H detection under varying chemical stimuli. *J. Mater. Chem. B* **2023**, *11* (27), 6296−6307.
(21) Fomin, M. A.; Dmitriev, R. I.; Jenkins, J.; Papkovsky, D. B.; Heindl, D.; König, B. Two-Acceptor Cyanine-Based Fluorescent Indicator for NAD(P)H in Tumor Cell Models. *ACS Sens.* **2016**, *1* (6), 702−709.
(22) Podder, A.; Murali, V. P.; Deepika, S.; Dhamija, A.; Biswas, S.; Maiti, K. K.; Bhuniya, S. NADH-Activated Dual-Channel Fluorescent Probes for Multicolor Labeling of Live Cells and Tumor Mimic Spheroids. *Anal. Chem.* **2020**, *92* (18), 12356−12362.
(23) Arachchige, D. L.; Dwivedi, S. K.; Jaeger, S.; Olowolagba, A. M.; Mahmoud, M.; Tucker, D. R.; Fritz, D. R.; Werner, T.; Tanasova, M.; Luck, R. L.; et al. Highly Sensitive Cyanine Dyes for Rapid Sensing of NAD(P)H in Mitochondria and First-Instar Larvae of Drosophila melanogaster. *ACS Appl. Bio Mater.* **2023**, *6* (8), 3199−3212.
(24) Arachchige, D. L.; Dwivedi, S. K.; Waters, M.; Jaeger, S.; Peters, J.; Tucker, D. R.; Geborkoff, M.; Werner, T.; Luck, R. L.; Godugu, B.; et al. Sensitive monitoring of NAD(P)H levels within cancer cells using mitochondria-targeted near-infrared cyanine dyes with optimized electron-withdrawing acceptors. *J. Mater. Chem. B* **2024**, *12* (2), 448−465.
(25) Cao, D. X.; Liu, Z. Q.; Verwilst, P.; Koo, S.; Jangjili, P.; Kim, J. S.; Lin, W. Y. Coumarin-Based Small-Molecule Fluorescent Chemosensors. *Chem. Rev.* **2019**, *119* (18), 10403−10519.
(26) Sun, Q. L.; He, D. M.; Zhang, L. S.; Li, Z. H.; Qu, L. B.; Sun, Y. Q. Coumarin-hemicyanine-based far-red to near-infrared fluorescent probes: A new generation of fluorescent probe design platform. *TrAC -Trends Anal. Chem.* **2023**, *167*, No. 117272.
(27) Sun, X. Y.; Liu, T.; Sun, J.; Wang, X. J. Synthesis and application of coumarin fluorescence probes. *Rsc Advances* **2020**, *10* (18), 10826−10847.
(28) Szwaczko, K. Fluorescent Coumarin-based Probe for Detection of Biological Thiols. *Curr. Org. Chem.* **2023**, *27* (15), 1329−1335.
(29) Xie, J. H.; Wang, L.; Su, X. Q.; Rodrigues, J. Coumarin-based Fluorescent Probes for Bioimaging: Recent Applications and Developments. *Curr. Org. Chem.* **2021**, *25* (18), 2142−2154.
(30) Pooja; Pandey, H.; Aggarwal, S.; Vats, M.; Rawat, V.; Pathak, S. R. Coumarin-based Chemosensors for Metal Ions Detection. *Asian. J. Org. Chem.* **2022**, *11* (12), No. e202200455.
(31) Tian, G.; Zhang, Z. X.; Li, H. D.; Li, D. S.; Wang, X. R.; Qin, C. G. Design, Synthesis and Application in Analytical Chemistry of Photo-Sensitive Probes Based on Coumarin. *Crit. Rev. Anal. Chem.* **2021**, *51* (6), 565−581.
(32) Wan, S. L.; Xia, S.; Medford, J.; Durocher, E.; Steenwinkel, T. E.; Rule, L.; Zhang, Y. B.; Luck, R. L.; Werner, T.; Liu, H. Y. A ratiometric near-infrared fluorescent probe based on a novel reactive cyanine platform for mitochondrial pH detection. *J. Mater. Chem. B* **2021**, *9* (25), 5150−5161.
(33) Xia, S.; Wang, J. B.; Bi, J. H.; Wang, X.; Fang, M. X.; Phillips, T.; May, A.; Conner, N.; Tanasova, M.; Luo, F. T.; et al. Fluorescent probes based on pi-conjugation modulation between hemicyanine and coumarin moieties for ratiometric detection of pH changes in live cells with visible and near-infrared channels. *Sensors and Actuators B-Chemical* **2018**, *265*, 699−708.
(34) Fang, M. X.; Adhikari, R.; Bi, J. H.; Mazi, W.; Dorh, N.; Wang, J. B.; Conner, N.; Ainsley, J.; Karabencheva-Christova, T. G.; Luo, F. T.; et al. Fluorescent probes for sensitive and selective detection of pH changes in live cells in visible and near-infrared channels. *J. Mater. Chem. B* **2017**, *5* (48), 9579−9590.
(35) Xu, J. H.; Bai, Y.; Ma, Q. J.; Sun, J. G.; Tian, M. J.; Li, L. K.; Zhu, N. N.; Liu, S. Z. Ratiometric Determination of Nitroxyl Utilizing a Novel Fluorescence Resonance Energy Transfer-Based Fluorescent Probe Based on a Coumarin-Rhodol Derivative. *Acs Omega* **2022**, *7* (6), 5264−5273.
(36) Johnson, R. E.; van der Zalm, J. M.; Chen, A. C.; Bell, I. J.; Van Raay, T. J.; Al-Abdul-Wahid, M. S.; Manderville, R. A. Unraveling the Chemosensing Mechanism by the 7-(Diethylamino)coumarin-hemicyanine Hybrid: A Ratiometric Fluorescent Probe for Hydrogen Peroxide. *Anal. Chem.* **2022**, *94* (31), 11047−11054.
(37) Paramasivam, M.; Kanvah, S. Rational Tuning of AIEE Active Coumarin Based alpha-Cyanostilbenes toward Far-Red/NIR Region Using Different pi-Spacer and Acceptor Units. *J. Phys. Chem. C* **2016**, *120* (20), 10757−10769.
(38) Cao, X. W.; Lin, W. Y.; Yu, Q. X.; Wang, J. L. Ratiometric Sensing of Fluoride Anions Based on a BODIPY-Coumarin Platform. *Org. Lett.* **2011**, *13* (22), 6098−6101.
(39) Gandioso, A.; Contreras, S.; Melnyk, I.; Oliva, J.; Nonell, S.; Velasco, D.; Garcia-Amoros, J.; Marchan, V. Development of Green/Red-Absorbing Chromophores Based on a Coumarin Scaffold That Are Useful as Caging Groups. *J. Org. Chem.* **2017**, *82* (10), 5398−5408.
(40) Gandioso, A.; Bresolí-Obach, R.; Nin-Hill, A.; Bosch, M.; Palau, M.; Galindo, A.; Contreras, S.; Rovira, A.; Rovira, C.; Nonell, S.; et al. Redesigning the Coumarin Scaffold into Small Bright Fluorophores with Far-Red to Near-Infrared Emission and Large Stokes Shifts Useful for Cell Imaging. *J. Org. Chem.* **2018**, *83* (3), 1185−1195.
(41) Rovira, A.; Gandioso, A.; Gonalons, M.; Galindo, A.; Massaguer, A.; Bosch, M.; Marchan, V. Solid-Phase Approaches for Labeling Targeting Peptides with Far-Red Emitting Coumarin Fluorophores. *J. Org. Chem.* **2019**, *84* (4), 1808−1817.
(42) Gandioso, A.; Palau, M.; Bresoli-Obach, R.; Galindo, A.; Rovira, A.; Bosch, M.; Nonell, S.; Marchan, V. High Photostability in Nonconventional Coumarins with Far-Red/NIR Emission through Azetidinyl Substitution. *J. Org. Chem.* **2018**, *83* (19), 11519−11531.
(43) Chen, J. H.; Liu, W. M.; Zhou, B. J.; Niu, G. L.; Zhang, H. Y.; Wu, J. S.; Wang, Y.; Ju, W. G.; Wang, P. F. Coumarin- and Rhodamine-Fused Deep Red Fluorescent Dyes: Synthesis, Photophysical Properties, and Bioimaging in Vitro. *J. Org. Chem.* **2013**, *78* (12), 6121−6130.
(44) Han, J. L.; Yang, S.; Wang, B. H.; Song, X. Z. Tackling the Selectivity Dilemma of Benzopyrylium-Coumarin Dyes in Fluorescence Sensing of HClO and SO2. *Anal. Chem.* **2021**, *93* (12), 5194−5200.
(45) Niu, G. L.; Liu, W. M.; Zhou, B. J.; Xiao, H. Y.; Zhang, H. Y.; Wu, J. S.; Ge, J. C.; Wang, P. F. Deep-Red and Near-Infrared Xanthene Dyes for Rapid Live Cell Imaging. *J. Org. Chem.* **2016**, *81* (17), 7393−7399.
(46) Fu, Z. H.; Han, X.; Shao, Y. L.; Fang, J. G.; Zhang, Z. H.; Wang, Y. W.; Peng, Y. Fluorescein-Based Chromogenic and Ratiometric Fluorescence Probe for Highly Selective Detection of Cysteine and Its Application in Bioimaging. *Anal. Chem.* **2017**, *89* (3), 1937−1944.
(47) Zhang, Y.; Bi, J.; Xia, S.; Mazi, W.; Wan, S.; Mikesell, L.; Luck, R. L.; Liu, H. A near-infrared fluorescent probe based on a FRET rhodamine donor linked to a cyanine acceptor for sensitive detection of intracellular pH alternations. *Molecules* **2018**, *23* (10), 2679.

https://doi.org/10.1021/acsabm.4c00595
ACS Appl. Bio Mater. 2024, 7, 5437−5451

(48) Austin, A.; Petersson, G. A.; Frisch, M. J.; Dobek, F. J.; Scalmani, G.; Throssell, K. A Density Functional with Spherical Atom Dispersion Terms. *J. Chem. Theory Comput.* **2012**, *8* (12), 4989−5007.
(49) *Gaussian 16, Revision A.03*; Gaussian, Inc.: Wallingford CT, 2016. (accessed).
(50) Cances, E.; Mennucci, B.; Tomasi, J. A new integral equation formalism for the polarizable continuum model: Theoretical background and applications to isotropic and anisotropic dielectrics. *J. Chem. Phys.* **1997**, *107* (8), 3032−3041.
(51) Casida, M. E.; Jamorski, C.; Casida, K. C.; Salahub, D. R. Molecular excitation energies to high-lying bound states from time-dependent density-functional response theory: Characterization and correction of the time-dependent local density approximation ionization threshold. *J. Chem. Phys.* **1998**, *108*, 4439−4449.
(52) Yanai, T.; Tew, D.; Handy, N. A new hybrid exchange-correlation functional using the Coulomb-Attenuating Method (CAM-B3LYP). *Chem. Phys. Lett.* **2004**, *393*, 51−57.
(53) GaussView, Version 6.0.16. *GaussView, Version 6.0.16*; Semichem Inc.: Shawnee Mission, KS, GaussView, Version 6.0.16. Semichem Inc. 2016. http://gaussian.com/g_prod/gv5.htm (accessed).
(54) Ince, C.; Coremans, J. M. C. C.; Bruining, H. A. In Vivo NADH Fluorescence. In *Oxygen Transport to Tissue XIV*, Erdmann, W.; Bruley, D. F., Eds.; Springer: US, 1992; pp 277−296.
(55) Dwivedi, S. K.; Arachchige, D. L.; Vohs, T.; Tang, J. N.; Usimaki, K.; Olowolagba, A. M.; Fritz, D. R.; Luck, R. L.; Werner, T.; Liu, H. Y. Near-infrared rhodol dyes bearing salicylaldehyde moieties for ratiometric pH sensing in live cells during mitophagy and under hypoxia conditions. *J. Mater. Chem. B* **2023**, *11* (13), 2852−2861.
(56) Mazi, W.; Yan, Y. N.; Zhang, Y. B.; Xia, S.; Wan, S. L.; Tajiri, M.; Luck, R. L.; Liu, H. Y. A near-infrared fluorescent probe based on a hemicyanine dye with an oxazolidine switch for mitochondrial pH detection. *J. Mater. Chem. B* **2021**, *9* (3), 857−863.
(57) Vegesna, G. K.; Janjanam, J.; Bi, J. H.; Luo, F. T.; Zhang, J. T.; Olds, C.; Tiwari, A.; Liu, H. Y. pH-activatable near-infrared fluorescent probes for detection of lysosomal pH inside living cells. *J. Mater. Chem. B* **2014**, *2* (28), 4500−4508.
(58) Wang, J. B.; Xia, S.; Bi, J. H.; Fang, M. X.; Mazi, W. F.; Zhang, Y. B.; Conner, N.; Luo, F. T.; Lu, H. P.; Liu, H. Y. Ratiometric Near-Infrared Fluorescent Probes Based On Through Bond Energy Transfer and π-Conjugation Modulation between Tetraphenylethene and Hemicyanine Moieties for Sensitive Detection of pH Changes in Live Cells. *Bioconjugate Chem.* **2018**, *29* (4), 1406−1418.
(59) Xia, S.; Fang, M. X.; Wang, J. B.; Bi, J. H.; Mazi, W.; Zhang, Y. B.; Luck, R. L.; Liu, H. Y. Near-infrared fluorescent probes with BODIPY donors and rhodamine and merocyanine acceptors for ratiometric determination of lysosomal pH variance. *Sens. Actuators B: Chem.* **2019**, *294*, 1−13.
(60) Xia, S.; Wang, J. B.; Bi, J. H.; Wang, X.; Fang, M. X.; Phillips, T.; May, A.; Conner, N.; Tanasova, M.; Luo, F. T.; et al. Fluorescent probes based on π-conjugation modulation between hemicyanine and coumarin moieties for ratiometric detection of pH changes in live cells with visible and near-infrared channels. *Sens. Actuators B: Chem.* **2018**, *265*, 699−708.
(61) Xia, S.; Zhang, Y. B.; Fang, M. X.; Mikesell, L.; Steenwinkel, T. E.; Wan, S. L.; Phillips, T.; Luck, R. L.; Werner, T.; Liu, H. Y. A FRET-Based Near-Infrared Fluorescent Probe for Ratiometric Detection of Cysteine in Mitochondria. *Chembiochem* **2019**, *20* (15), 1986−1994.
(62) Qi, X.; Tester, R. F. Lactose, Maltose, and Sucrose in Health and Disease. *Mol. Nutr. Food Res.* **2020**, *64* (8), No. e1901082.
(63) Lin, Y. J.; Wang, Y.; Li, P. F. Mutual regulation of lactate dehydrogenase and redox robustness. *Front. Physiol.* **2022**, *13*, No. 1038421.
(64) Augoff, K.; Hryniewicz-Jankowska, A.; Tabola, R. Lactate dehydrogenase 5: An old friend and a new hope in the war on cancer. *Cancer Lett.* **2015**, *358* (1), 1−7.
(65) Karstadt, M. L. Regulation of carcinogenic food additives in the United States. *Eur. J. Oncol.* **2009**, *14* (2), 79−92.
(66) Belton, K.; Schaefer, E.; Guiney, P. D. A Review of the Environmental Fate and Effects of Acesulfame-Potassium. *Integrated Environmental Assessment and Management* **2020**, *16* (4), 421−437.
(67) MacLean, A.; Legendre, F.; Appanna, V. D. The tricarboxylic acid (TCA) cycle: a malleable metabolic network to counter cellular stress. *Crit. Rev. Biochem. Mol. Biol.* **2023**, *58* (1), 81−97.
(68) Gu, X.; Yan, Y.; Novick, S. J.; Kovach, A.; Goswami, D.; Ke, J. Y.; Tan, M. H. E.; Wang, L. L.; Li, X. D.; de Waal, P. W.; et al. Deconvoluting AMP-activated protein kinase (AMPK) adenine nucleotide binding and sensing. *J. Biol. Chem.* **2017**, *292* (30), 12653−12666.
(69) Burh, A.; Batra, S.; Sharma, S. Emerging Facts on Chronic Consumption of Aspartame as Food Additive. *Curr. Nutr. Food Sci.* **2021**, *17* (7), 690−698.
(70) Kirkland, D.; Gatehouse, D. Aspartame: A review of genotoxicity data. *Food Chem. Toxicol.* **2015**, *84*, 161−168.
(71) Holecek, M. Aspartic Acid in Health and Disease. *Nutrients* **2023**, *15* (18), 4023.
(72) Cersosimo, R. J. Oxaliplatin-associated neuropathy: A review. *Ann. Pharmacother.* **2005**, *39* (1), 128−135.
(73) Jardim, D. L.; Rodrigues, C. A.; Novis, Y. A. S.; Rocha, V. G.; Hoff, P. M. Oxaliplatin-related thrombocytopenia. *Ann. Oncol.* **2012**, *23* (8), 1937−1942.
(74) Stein, A.; Arnold, D. Oxaliplatin: a review of approved uses. *Expert Opin. Pharmacother.* **2012**, *13* (1), 125−137.
(75) Gnoni, A.; Russo, A.; Silvestris, N.; Maiello, E.; Vacca, A.; Marech, I.; Numico, G.; Paradiso, A.; Lorusso, V.; Azzariti, A. Pharmacokinetic and Metabolism Determinants of Fluoropyrimidines and Oxaliplatin Activity in Treatment of Colorectal Patients. *Curr. Drug Metab.* **2011**, *12* (10), 918−931.

https://doi.org/10.1021/acsabm.4c00595
ACS Appl. Bio Mater. 2024, 7, 5437−5451